Synthesis and Measurement of DBE Exceptional Points in Substrate-Integrated Waveguides

Tianyu Zheng, *Student Member, IEEE*, Massimiliano Casaletti, *Senior Member, IEEE*,
Ahmed F. Abdelshafy, *Student Member, IEEE*, Filippo Capolino, *Fellow, IEEE*,
Zhuoxiang Ren, *Senior Member, IEEE*, and Guido Valerio, *Senior Member, IEEE*

Abstract— This article proposes a method to engineer degenerate band-edge conditions in periodic substrate-integrated waveguides (SIWs). A degenerate band edge (DBE) is a fourth-order exceptional point originating from the coupling of four Floquet–Bloch modes; it leads to a dispersion relation flatter than a regular band edge (RBE) and is suitable to design slow wave structures and high Q-factor resonators. Design guidelines to achieve a DBE point are given based on Bloch analyses of unit cells. An oblique line of vias in SIW is proposed to form a suitable modal coupling between adjacent waveguides enabling a degenerate band-edge condition. The effect of losses and the robustness to parameter variations are discussed by means of rigorous Bloch analyses. A unit cell showing the best behavior concerning the losses and geometric tolerances is selected and prototypes of finite-length resonators are realized. Measurements validate simulated results and confirm the typical N^5 scaling of the loaded Q-factor to the number of cells N of the resonator.

Index Terms— Degenerate band edge (DBE), dispersive analysis, electromagnetic bandgap, periodic structures, slow wave structure, substrate integrated waveguide.

I. INTRODUCTION

IN RECENT years, research on degenerate band edge (DBE) showed a feasible way to obtain very strong

Tianyu Zheng was with Sorbonne Université, CNRS, Laboratoire de Génie Electrique et Electronique de Paris, 75252 Paris, France. He is now with the Institute of Electrical Engineering, Chinese Academy of Science, Beijing 100190, China (e-mail: zhengtianyu@mail.iee.ac.cn).

Massimiliano Casaletti, Zhuoxiang Ren, and Guido Valerio are with Sorbonne Université, CNRS, Laboratoire de Génie Electrique et Electronique de Paris, 75252 Paris, France, and also with Centrale Supélec, CNRS, Laboratoire de Génie Electrique et Electronique de Paris, Université Paris-Saclay, 91192 Gif-sur-Yvette, France (e-mail: massimiliano.casaletti@sorbonne-universite.fr; zhuoxiang.ren@sorbonne-universite.fr; guido.valerio@sorbonne-universite.fr).

Ahmed F. Abdelshafy is with the Department of Electrical Engineering and Computer Science, University of California, Irvine, CA 92697 USA (e-mail: abdelsha@uci.edu).

Filippo Capolino is with the Department of Electrical Engineering and Computer Science, University of California, Irvine, CA 92697 USA, and also with the Department of Communications and Signal Theory, University Carlos III of Madrid, 28911 Leganés, Madrid, Spain (e-mail: f.capolino@uci.edu).

Color versions of one or more figures in this article are available at https://doi.org/10.1109/TMTT.2022.3200102.

Digital Object Identifier 10.1109/TMTT.2022.3200102

resonances in microwave and optical waveguides. DBE occurs when four eigenmodes coalesce together [1]. This coupling can be obtained by designing a suitable periodic coupling between uniform transmission lines; as shown at first in photonic crystals [2], the coupling among plane waves with orthogonal polarizations is achieved by means of anisotropic layers.

After the pioneering work by Figotin and Vitebskiy more than 15 years ago [1], [2], it was demonstrated that this phenomena can also be obtained by other mechanisms than in photonic crystals, as shown in several designs recently proposed at microwave frequencies, such as the double ladder lumped circuit [3], [4], coupled microstrip lines [5], [6], [7], [8], [9], [10], circular waveguide [11], [12], and in optics, like silicon ridge waveguides [13], [14], coupled resonator optical waveguide [15], [16], multilayer dielectric resonator [17], [18], multilayer dielectric antenna [19], [20], [21], and coupled transmission line array antenna [22]. Proposed applications so far are in high-power oscillator [23], [24], oscillators [3], [25], pulse compression device [26], low threshold switching [27], and laser [28].

While a regular band edge (RBE) exists in every lossless periodic structure and is locally characterized by a quadratic dispersion curve [1], a DBE is a much more difficult condition to achieve. Let the Bloch wavenumber of a mode of the periodic structure be $k = \beta - j\alpha$, β being the phase constant, and α the attenuation constant. Due to the fourth-order coalescence, near the DBE the dispersion relation between the frequency f and β is described by a quartic curve [2]

$$f - f_d = a(\beta - \beta_d)^4 \tag{1}$$

where a is a constant depending on the waveguide physical and geometrical configuration, f_d is the DBE frequency and $\beta_d = \pi/d$ is the Brillouin zone edge [see Fig. 1(a)]. The quartic dispersion behavior of DBE provides a larger reduction of group velocity near the Brillouin edge if compared to RBE. In fact, according to (1), not only the group velocity $v_p = 2\pi \partial f/\partial \beta$, but also the first and second derivatives of the group velocity are zero at the DBE. Therefore, the group velocity is extremely low near the DBE frequency, for various wavenumbers. This leads to a giant resonance and a high-quality factor for DBE-based truncated lines [1] composed of N unit cells. Their loaded Q-factor is proportional to N^5, whereas a N^3 scaling is found in RBE-based truncated lines [11]. The rapid growth of Q-factors in DBE structures is particularly attractive for the
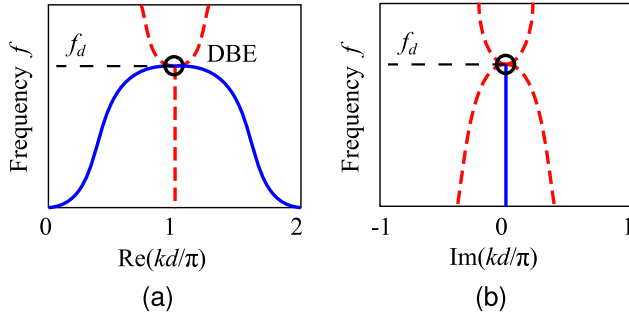
Fig. 1.   Dispersion diagram of a periodic line of period d exhibiting a DBE. Propagating modes (blue lines) and evanescent modes (red dashed lines). (a) Phase constant. (b) Attenuation constant.

design of high Q-factor resonators in compact size. Of course, the presence of losses eventually prevents the fast increase of Q-factor for long DBE resonators; however, this factor can be compensated by introducing distributed elements providing gain to each cell [29].

These results motivate the synthesis of DBE in periodic substrate-integrated waveguide (SIW) structures, which have the advantage of being low-cost, compact, are suitable for integration at millimeter-wave frequencies, and suppress radiation losses [30]. DBEs in SIW are therefore attractive for the design of integrated resonators with very high-quality factors and can pave the way to the realization of robust oscillators at high frequencies [29]. Furthermore, opening slots on the upper SIW plate would allow for the design of ultra-sensitive sensors based on the directive radiation of the periodic resonant guided wave. Unfortunately, while in most of the previously designed DBE structures wave propagation occurs mainly or partly in the air, propagation in SIW occurs fully through a dielectric media and is confined by very close conducting plates. The impact of dielectric and conductor losses is then expected to be a critical issue in the synthesis of DBE in SIW, and it is here investigated.

In this article, we achieve the synthesis of DBE in periodic SIW structures by means of different spatial distributions of via holes for the suitable coupling between two adjacent waveguides. In order to validate the existence of a DBE, a Bloch analysis is performed, by describing the unit cell as a four-port network whose transmission matrix is computed using full-wave simulations. The eigenvalues of the transmission matrix are related to the complex wavenumbers of the Bloch modes, including both the phase and the attenuation constants. Some preliminary simulated studies were performed in [31] and [32], and simulations of an air-filled SIW, capable of reducing losses, were performed in [33]. Here, we give a complete theoretical and experimental study of the dielectric-filled SIW, whose fabrication is easier than the air-filled one in [33]. We start by presenting the unit cell treated in [31] since this will help to follow the progressive simplification of the structure and the properties of new unit cells. In fact, we propose a novel unit-cell topology whose size is more compact than those in [31] and [32] and it is more robust with respect to losses and geometrical parameters compared to those in [31], [32], and [33]. Furthermore, we validate for

the first time the study with measurements of SIW cavities. In Section II, we propose four different SIW unit-cell designs to achieve the DBE. The design named "corner cell" is compact in size and is shown to be more robust to the perturbation of geometric parameters and losses. In Section III, we study the resonant behavior of truncated SIWs-DBE lines, design a feeding transition for measurements, and present the fabrication process and experimental results of SIWs-DBE lines.

II. DESIGN OF SIW DBE UNIT CELLS

We present the Bloch analyses of three different unit cells in SIW technology, suitably designed to support a DBE resonance. For the convenience of the reader, these cells are named as "double-coupler cell," "single-coupler cell," and "corner cell," respectively.

Note that the DBE fourth-order condition should be verified in the complex plane of the Bloch wavenumber $k = \beta - j\alpha$. At the DBE frequency, both the β and α of four Bloch modes coalesce. Therefore, eigenvalue analyses of common commercial software, computing usually the phase constant only, are not suitable for this study. All Bloch analyses presented here are then based on the computation of the eigenvalues of a generalized transfer-matrix [6] where the unit cell is a *four-port network* composed of a pair of 1-D periodic coupled transmission lines. The frequency-domain finite-element Ansys HFSS software is used to perform full-wave simulations of the cells and extract their 4×4 scattering matrices $\underline{\mathbf{S}}$. Each $\underline{\mathbf{S}}$ matrix is converted into a transfer matrix $\underline{\mathbf{T}}$; the eigenvalues of $\underline{\mathbf{T}}$ are the four wavenumbers of the Bloch modes supported by the cell [34]. In order to verify the coalescence of the four wavenumbers, we compute a coalescence parameter D_H, measuring the distance among the four 4-D eigenvectors $\mathbf{\Psi}_n$ of the transfer matrix at a given frequency [6]

$$D_H = \frac{1}{6} \sum_{\substack{m,n=1 \\ m \neq n}}^{4} \sin(\theta_{mn}), \quad \cos(\theta_{mn}) = \frac{\Re e\{\langle \mathbf{\Psi}_n, \mathbf{\Psi}_m \rangle\}}{\|\mathbf{\Psi}_n\| \cdot \|\mathbf{\Psi}_m\|} \quad (2)$$

where $\langle a, b \rangle$ is the Hermitian inner product and $\|a\| = \sqrt{\langle a, a \rangle}$. A null coalescence parameter at a given frequency is equivalent to a fourth-order coalescence at that frequency.

All the analyses are at first performed in the absence of losses since a perfect degeneracy is not observable in lossy cells. The impact of losses is evaluated on the optimized structures.

A. Unit Cell With Double Coupling ("Double-Coupler Cell")

The first unit cell proposed follows the physical mechanism found in the DBE circular waveguides, where two misaligned elliptical irises introduce an asymmetrical coupling between degenerate waveguide modes [11]. Instead of two degenerate modes in the same waveguide, we use here two identical adjacent SIWs waveguides supporting the same fundamental TE$_{10}$ mode. Within a cell, the waveguides are coupled with two coupling elements, each composed of an oblique line of vias and a coupling gap.
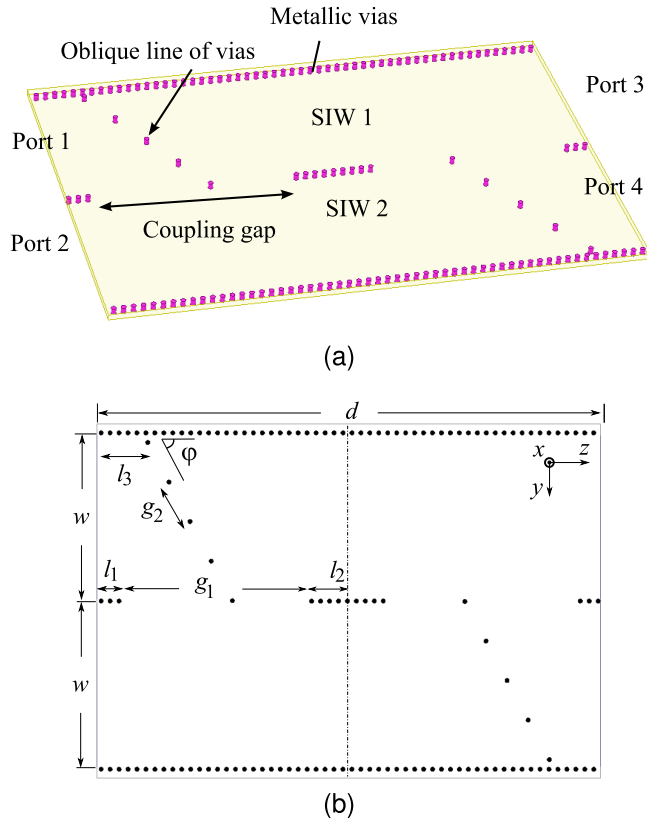
(a)

(a)

(b)

Fig. 2. Geometry of the "double coupler" SIW-DBE unit cell design. (a) 3-D view. The magenta dots are metallic vias drilled in the dielectric substrate (in light yellow). (b) Dimensions (top view).
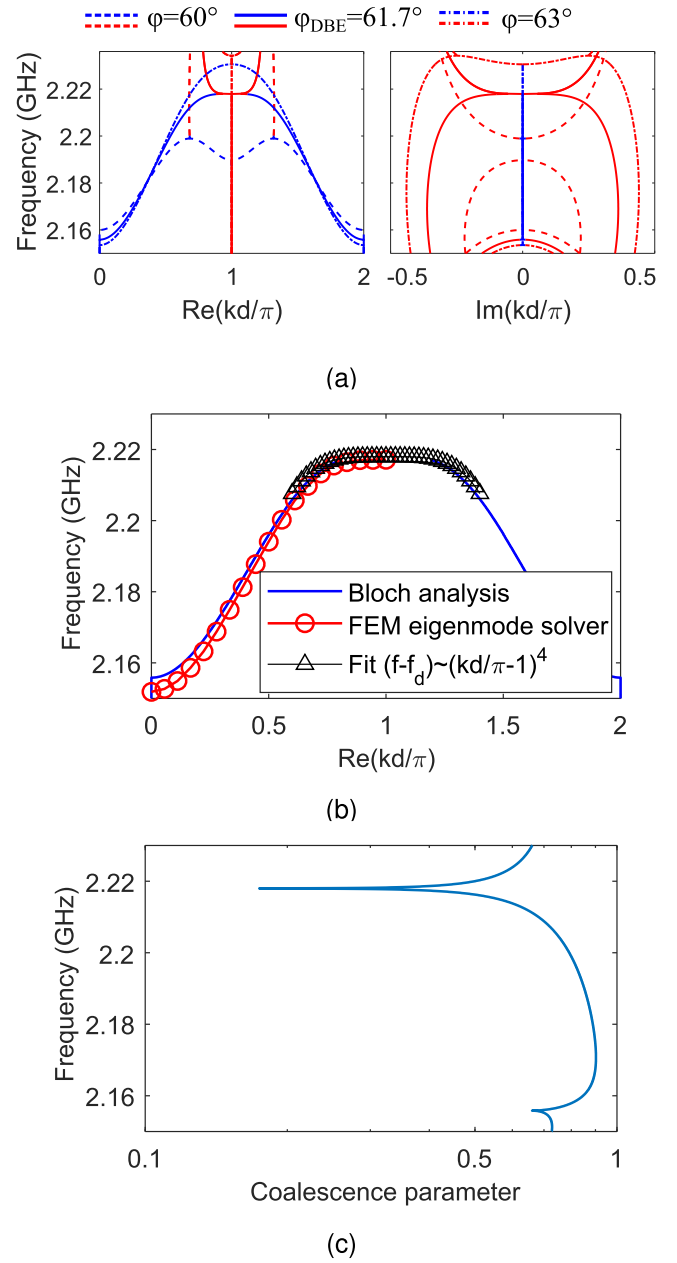

(b)

(c)

Fig. 3. Dispersion diagram of the lossless "double-coupler cell." (a) Dispersion relations for different misalignment angles (propagating modes in blue curves and evanescent modes in red curves). (b) Dispersion diagram of the purely real-wavenumber mode when the DBE is achieved. (c) Level of the dip of the coalescence parameter reveals the closeness to an ideal DBE condition.

The 3-D view of the "double-coupler" is shown in Fig. 2(a) and its dimensions are shown in Fig. 2(b). All distances in the pictures are measured between the centers of the vias involved, except the period of the structure d which is taken between the cell edges. The parameters are chosen in order to have a DBE around 2 GHz. The width w of each waveguide is 30 mm, the period d is 90 mm and the thickness of the substrate is 1 mm. In the parallel rows of vias of the SIWs, the radius is 0.8 mm and the distance between consecutive via is 1.6 mm. The lengths of the middle rows of vias are $l_1 = 4$ mm and $l_2 = 6.8$ mm, respectively. The length of each coupling gap is $g_1 = 34.2$ mm. The length from the starting point of the oblique line to the left border $l_3 = 9.1$ mm and the distance between the oblique vias $g_2 = 8$ mm. The material of the substrate is Rogers RO3010, whose relative permittivity is 10.2. The vias and the ground plane are perfect electric conductors (PECs), and, at this stage, the structure is assumed to be lossless.

The couplers in the unit cell should be suitably designed in order to create a DBE. The oblique line angle φ and position l_3 are the two main parameters capable of a finetuning leading to a DBE. In Fig. 3(a), we show the dispersion diagrams of the periodic structure for three different misalignment angles, $\varphi = 60°$, $\varphi = 61.7°$ and $\varphi = 63°$, where the oblique line position is fixed to $l_3 = 9.1$ mm. As explained at the beginning of the section, these simulations have been performed with Ansys HFSS, which computes the 4×4 **S** matrix of a single

cell. In each simulation, the four access ports are excited as 'wave ports' with their fundamental TE$_{10}$ mode. The **S** matrix is transformed into a **T** matrix, whose eigenvalues are related to the wavenumbers of the Bloch modes supported by the periodic waveguides.

By choosing arbitrary misalignment angles a RBE is easily obtained as expected, while achieving a DBE condition requires a finer tuning. When $\varphi = 60°$ two transition points from propagating to evanescent mode are visible (at around 2.2 GHz) inside the Brillouin zones shown in the figure, a condition known as split band edge. These are second-order

degeneracies, since two propagating (real) modes coalesce at 2.2 GHz into two complex conjugate modes arising at higher frequencies. When φ is increased from 60° to 61.7°, the two second-order degeneracies get closer, the dispersion curve of propagating modes becomes more flat, and the four Bloch modes tend to degenerate together at the same frequency (at 2.218 GHz). When the misalignment angle is increased, for example to 63°, the dispersion curves of the propagating and evanescent modes separate from each other, and no DBE occurs.

In conclusion, the DBE point exists for $\varphi_{\text{DBE}} = 61.7°$; the dispersion curve of this periodic structure is shown in Fig. 3(b). Here, we compare the phase constant computed with our Bloch analysis with the one computed by the FEM eigensolver and a fit of a quartic curve of the kind (1). In order to verify that a DBE is achieved, we compute the coalescence parameter D_H in Fig. 3(c). This parameter represents the sum of all the angles between the four degenerate eigenvectors [6] and it is also used to measure how a system is close to its ideal DBE. A zero at the DBE frequency confirms the coalescence of the four eigenvectors as expected.

The impact of losses should be now considered, since losses prevent a perfect coalescence of Bloch modes [35], i.e., the existence of the DBE point. Losses in SIW include conductor losses, dielectric losses, and leakage through the lateral via wall. The latter is here negligible since the via wall satisfies the design rules in [36], and it is anyway always taken into account in simulations since the structure is terminated with lateral PML boundary conditions. Dielectric losses are determined by the loss tangent of the substrate (3.5×10^{-3} for Rogers RO3010), and conductor losses are considered for copper. The dispersion diagrams with losses are shown in Fig. 4(a). A smoother behavior is now observed close to the frequency where the DBE occurs in the lossless case. Furthermore, we also consider conductor and dielectric losses separately: we can see that dielectric losses are the main contribution to total losses. The coalescence parameter results in Fig. 4(b) confirm this conclusion: while the coalescence parameter of the lossless case is zero, it stays above 0.5 after considering losses. The coalescence parameter including only the dielectric losses is larger than the one considering only the conductor losses, which confirms that the dielectric losses are the main source of losses.

A first step in the minimization of losses is the use of a thicker substrate [37]. In Fig. 5, the "double-coupler cell" structure is simulated with the same substrate material Rogers RO3010 but different thicknesses, and the results confirm that a DBE point is more closely approached with a thick substrate.

B. Compact Unit Cell With One Coupler ("Single-Coupler Cell")

The previous design gave relatively good results in achieving DBE, but we aim at further simplifying the unit cell by reducing its size and the number of vias, to make it more robust with respect to losses and possibly to imperfections and variations of geometrical parameters. We use here two adjacent waveguides having only one coupler element in the
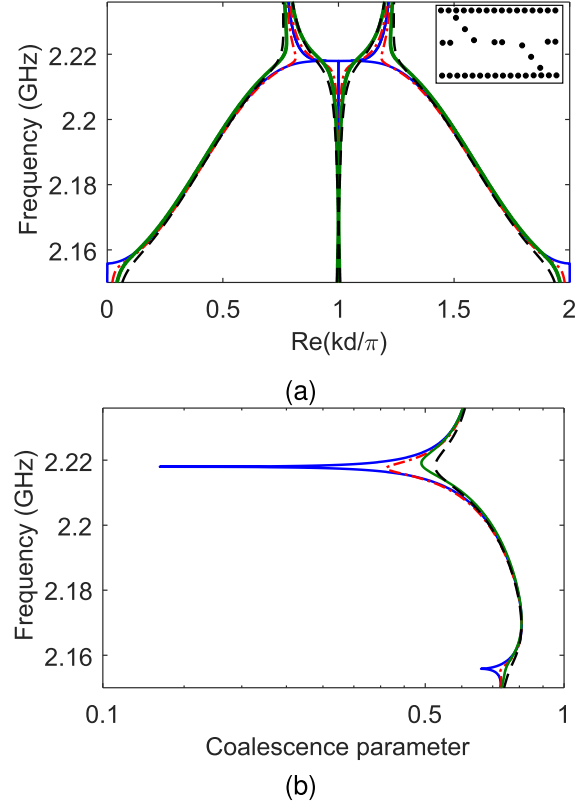

Fig. 4. Losses influence on DBE of "double-coupler cell" design. Four different cases are considered: lossless (blue line), only conductor losses (red dashed line), only dielectric losses (green line), and both conductor and dielectric losses (black dashed line). (a) Dispersion diagram. (b) Coalescence parameter.

unit cell (i.e., only one coupling gap and only one oblique line of vias).

This results in a more compact design with only one oblique line of vias is shown in Fig. 6. Here we only use one coupling gap in each cell, and the cell size is 40 mm × 44.8 mm. The SIW's width $w = 20$ mm and the period $d = 44.8$ mm (i.e., roughly half of the period of the previous unit cell). To prevent lateral leakage, the via diameter is set to 0.4 mm and their separation is 0.8 mm. The thickness of the substrate is 1.28 mm and the material of the substrate is again Rogers RO3010. The coupling-gap length is $g_c = 26.4$ mm. The distance between vias in the oblique line $g_o = 7$ mm. After optimization, the angle is $\varphi_{\text{DBE}} = 71°$ and the length is $g_d = 11.3$ mm.

The dispersion diagram of the lossless unit cell is shown in Fig. 7(a) where the DBE point is at 2.516 GHz. The coalescence parameter null in Fig. 7(b) confirms the DBE requirement. The impact of losses confirms again that a perfect DBE disappears in a lossy structure.

C. Unit Cell Robust to Perturbations ("Corner Cell")

Here, we propose the last design to further ease the matching of the periodic line once a truncated line is considered and a feeding waveguide is assumed on one side of a truncated line. In fact, once a truncated structure composed of a finite number of cells is considered as in [6], the DBE can be excited feeding
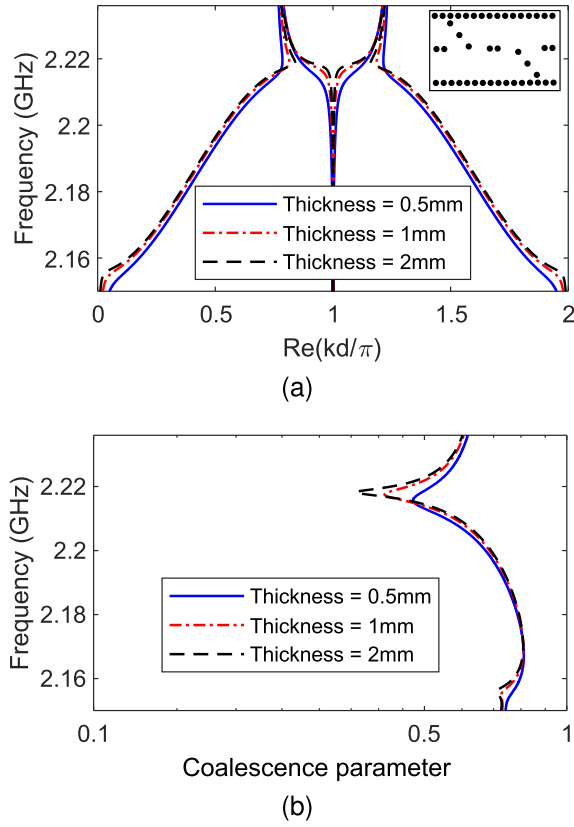
Fig. 5. Thickness influence on DBE of "double-coupler cell" design. Only conductor losses are considered. (a) Dispersion diagram. (b) Coalescence parameter.
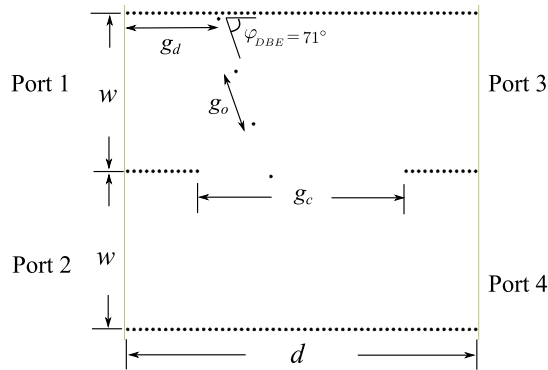

Fig. 7. Dispersion diagram of "single-coupler cell." The DBE is located at 2.516 GHz. Lossless (blue line), only conductor losses (red dashed line), only dielectric losses (green line), and both conductor and dielectric losses (black dashed line). (a) Dispersion diagram. (b) Coalescence parameter.

Fig. 6. Geometry of the "single-coupler cell."

Fig. 8. Geometry of "corner cell."

only one of the two parallel waveguides, while the adjacent one is shorted. The same is done on the opposite end of the line. Having this in mind, we adopt a geometry where the ports which will be used for the feeding are minimally perturbed by the periodic vias, still assuring the coupling required for the DBE conditions. An interesting property of this third unit cell is a far more robustness to the perturbation of the oblique vias direction and to losses, with respect to previous designs.

The new design is shown in Fig 8; it includes two short oblique lines of vias near port 1 and 3 and a coupling gap between the waveguides. The width of each waveguide $w = 21.5$ mm; the period $d = 34.8$ mm; the lengths labeled in the
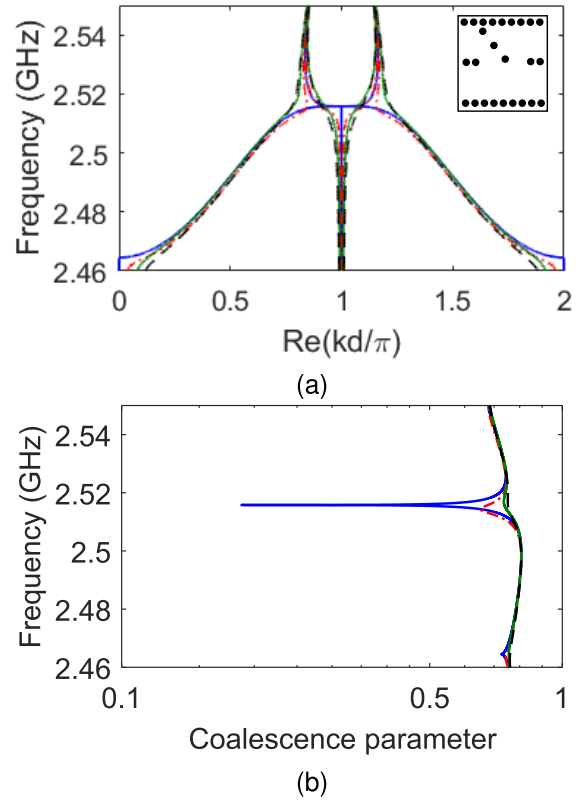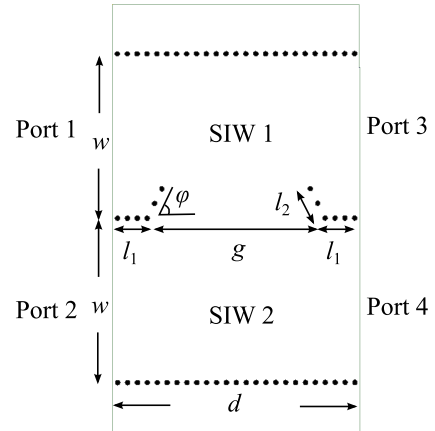
figures are $l_1 = 4.5$ mm and $l_2 = 4.5$ mm; the gap length $g = 25.8$ mm; the angle $\varphi = 76°$. The diameter of the via is 0.6 mm, the separation between vias is 1.2 mm. The substrate is 1.28 mm Rogers RO3010. This is the unit cell with the smallest period among the three presented in this section.

The dispersion diagram of the lossless corner cell is shown in Fig. 9(a) which shows that a DBE is achieved at 2.5 GHz (the same frequency as in the previous "single-coupler cell") for an angle $\varphi = 76°$ (the angle of the oblique rows of vias). Fig. 9(b) confirms that the coalescence parameter does
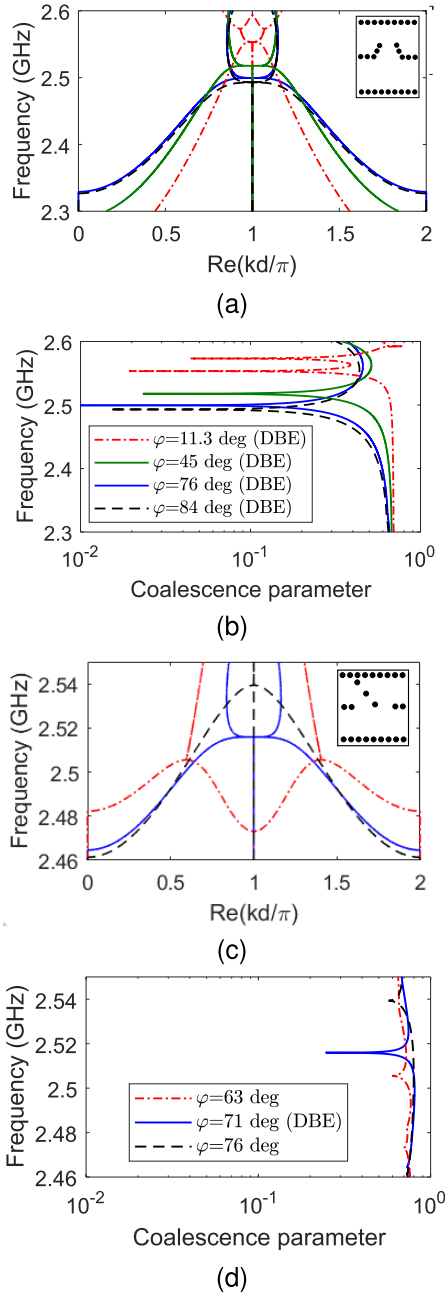
Fig. 9. Influence of the angle φ of oblique vias on the DBE for two configurations, the "corner cell" and the 'single-coupler cell," where φ is shown in Figs. 8 and 6, respectively. (a) Dispersion diagram of the "corner cell" design. (b) Coalescence parameter of the "corner cell" design. (c) Dispersion diagram of the "single-coupler cell." (d) Coalescence parameter of the "single-coupler cell." In summary, the "corner cell" provides a better DBE that can be even tuned by varying φ.

Fig. 10. Dispersion diagrams of the "corner cell" design with different values of l_1 and l_2. (a) $l_1 = 4.5$ mm $+ \Delta l_1$, with Δl_1 given in the label. $\Delta l_1 = 0$ is shown in Fig. 9. (b) $l_2 = 4.5$ mm $+ \Delta l_2$, with Δl_2 given in the label. $\Delta l_2 = 0$ is shown in Fig. 9.

go to zero at 2.5 GHz if $\varphi = 76°$. The most interesting feature of this new design is its increased robustness to the perturbation of the oblique lines of vias. We compare the influence of a perturbation of φ on the dispersion diagram of this design [Fig. 9(a) and (b)] and of the "single-coupler cell" [Fig. 9(c) and (d)]. From Fig. 9(a) and (c), we can see that, for a wide range of angles (from 11.3° to 84°), the new compact design can always achieve a DBE condition, and the effect of the φ variation only cause a small frequency shift. On the
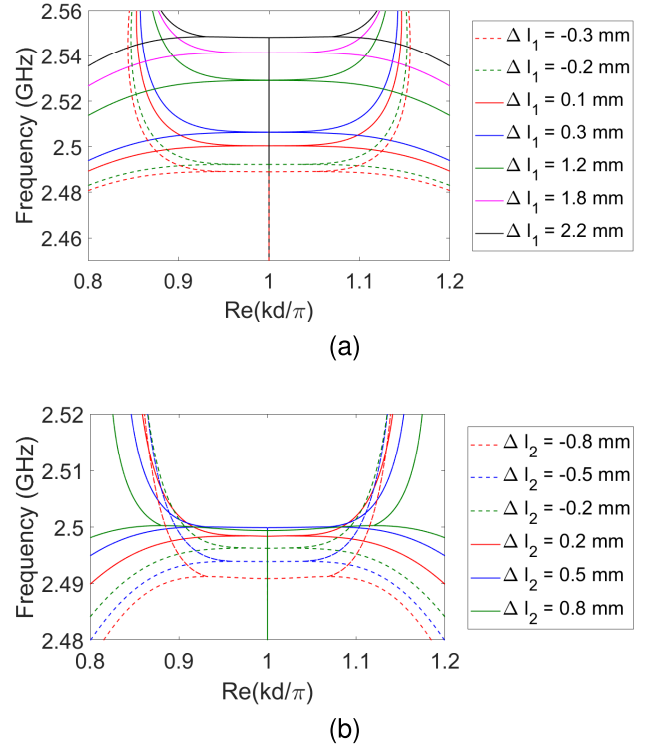
contrary, the "single-coupler cell" achieves a DBE only for a single value of φ. This phenomenon was already discussed regarding the "double-coupler cell": in Fig. 3, we observed the loss of DBE for small perturbation of 1.7° and 1.3°. In both the "double-coupler cell" and the "single-coupler cell," a small perturbation of φ leads to the loss of the fourth-order degeneracy, converted into two separate second-order degeneracies. The coalescence parameters in Fig. 9(b) and (d) confirm this conclusion.

In Fig. 10, we show the impact of the variation of the parameters l_1 and l_2 on the dispersion diagram of the "corner cell." When modifying the length l_i, we keep the same number of metallic pins and distribute them equally spaced along the new length. We see that the DBE is maintained under small variations Δl_i of $l_i, i = 1, 2$ (-0.3 mm $\leq \Delta l_1 \leq 2$ mm and -0.5 mm $\leq \Delta l_2 \leq 0.8$ mm) (larger variations would eventually lead to a splitting of the DBE into two RBEs). These limiting values are above the typical manufacturing precision of PCB technology. Interestingly, small variations of these lengths not only preserve the DBE but do not move it significantly in frequency. The robustness of the "corner cell" is particularly useful, since it allows to adjust the DBE frequency by changing the φ parameter angle, and to tolerate reasonable variations of the geometrical parameters l_1, l_2 in such a way that the resonance is not lost.

Another important result concerns the effect of losses, shown in Fig. 11. Losses due to the copper and the usual RO3010 substrate are taken into account in the dispersion diagram of Fig. 11(a). A graphical visualization of the figure
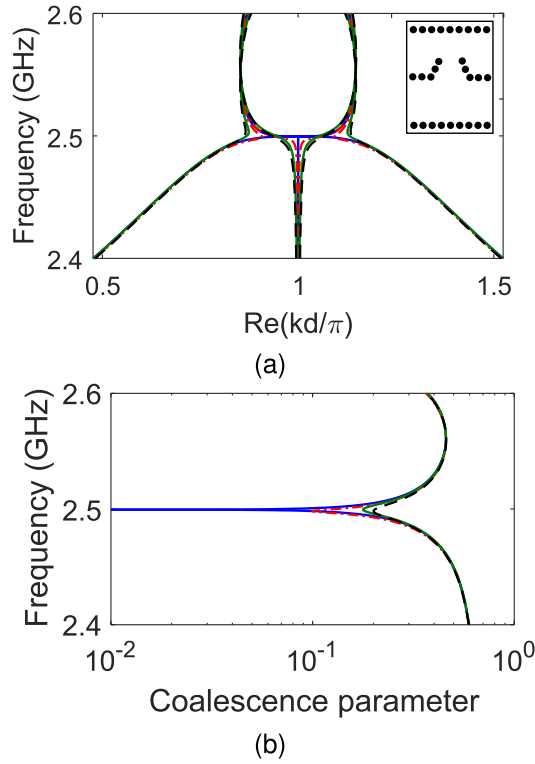
Fig. 11. Dispersion of the "corner cell" in different cases: lossless (blue line), only conductor losses (red dashed line), only dielectric losses (green line), and both conductor and dielectric losses (black dashed line). (a) Dispersion diagram. (b) Coalescence parameter.

shows a much smaller impact of losses on the resonance. This is quantitatively confirmed by looking at the coalescence parameter in Fig. 11(b). The lossy coalescence parameter of the "corner cell" is the smallest among all the cells presented: a minimum value of 0.2 is reached, while the other two cells lead to minimum values larger than 0.5. In conclusion, this new compact "corner cell" design has a similar but smaller size of the "single-coupler cell," it is more robust to the perturbation of the oblique rows of vias, and suffers less of the presence of losses. For this reason, we select this topology for an additional study with a low-loss substrate, in order to further improve its performance in the presence of losses.

D. Analysis of Dielectric Losses

As shown in the three previous designs, sensitivity to losses in SIW structures limits the synthesis of a pure DBE occurrence in real structures. It should be noticed that the study of losses in SIW-based designs are more important than with respect to other DBE technologies previously studied (microstrips, circular waveguides). In fact, for SIWs, wave propagation occurs inside a dielectric medium and between two very close metallic plates.

In all previous designs, dielectric losses are dominant among the total losses. For this reason, we investigate here the impact on the DBE resonances of lower dielectric losses in the three unit cells. We modify the Rogers loss tangent used in the previous cells (3.5×10^{-3}) with a lower loss substrate (6×10^{-4}). This value is taken from the Neltec NY9208 substrate, a candidate for the fabrication of the low-loss

prototype presented in Section III. The Neltec substrate has also a different dielectric constant and would also require modifying the complete designs of the cells. However, in order to establish a fair comparison with previous results, at this point we modify only the tangent loss and keep all the other geometrical and physical parameters constant.

In Table I we show the three designs with the two levels of losses. In each case, we compute the minimum of the coalescence parameter as a measure of the proximity of the eigenvectors which should rigorously degenerate in the lossless case. The coalescence parameter of all three designs are reduced when using the lower-loss-tangent substrate, which confirms a better approximation of the DBE condition. Again, the closest DBE condition is achieved by the "corner cell', whose coalescence parameter is one-third of the "double-coupler cell" and almost one-fifth "single-coupler cell."

III. SIW HIGH-Q TRUNCATED DBE-RESONATOR

Three topologies of SIWs-DBE unit cells have been proposed in Section II. Among them, the "corner cell" design is the most compact and robust both to geometric perturbation of oblique vias and to dielectric losses. Furthermore, one single parameter (the angle φ) allows tuning the resonance frequency by keeping a DBE condition. A SIW high-Q resonator is therefore proposed in this section based on the "corner cell" topology, properly modified to minimize the losses.

A. Low-Loss Corner-Cell Unit Cell

We propose a new design based on the corner-cell topology, employing a Neltec NY9208 substrate, whose relative dielectric constant is $\epsilon_r = 2.08$ and loss tangent is 6×10^{-4}. We keep the size of the cell similar to the one used in Section II-C, and set the DBE frequency around 6 GHz. Thanks to the robustness with respect to the angle φ discussed after Fig. 11, the new design is simply achieved by means of a geometric scaling taking into account the new dielectric and the new DBE frequency, followed by a fine tuning of φ, which leads to a precise definition of the DBE frequency. The width of both waveguides is $w = 20$ mm; the period $d = 30$ mm; the coupling gap length $g = 21.6$ mm; the length $l_1 = 4.2$ mm; the length $l_2 = 4$ mm; the angle $\varphi = 45°$. The diameter of the via is 0.6 mm, the separation between two vias is 1.2 mm. The thickness of the substrate is 1.524 mm.

The dispersion relation of this new cell is shown in Fig. 12(a). The DBE point is at 6.17 GHz and its existence is confirmed by a null of the coalescence parameter in Fig. 12(b). If compared with the results using the ROGERS substrate in Section II, the contribution of dielectric losses is now decreased and comparable to the conductive losses. This confirms that the loss tangent of the new substrate is sufficiently low and that a lower loss tangent would not significantly enhance the performance of the design.

B. Resonances in SIW Cavities

We analyze the resonances in an SIW cavity made of a chain of N unit cells of the same kind as described in Section II-C.

TABLE I

COALESCENCE PARAMETER OF THE LOSSY SIW UNIT CELLS AT THE DBE FREQUENCY ($\epsilon_r = 10.2$)

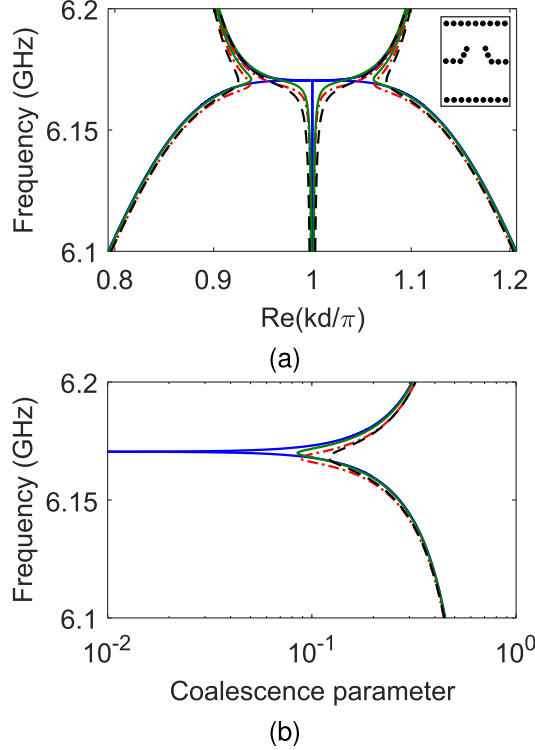| Unit Cell Type	DBE Frequency (GHz)	Coalescence parameter (loss tangent: 3.5×10^{-3})	Coalescence parameter (loss tangent: 6×10^{-4})
"double-coupler cell"	2.218	5.25×10^{-1}	4.45×10^{-1}
"single-coupler cell"	2.516	7.53×10^{-1}	6.95×10^{-1}
"corner cell"	2.500	2.10×10^{-1}	1.44×10^{-1}

Fig. 12. Dispersion diagram of "low-loss corner-cell" design. The DBE frequency is at 6.17 GHz. Lossless (blue line), only conductor losses (red dashed line), only dielectric losses (green line), and both conductor and dielectric losses (black dashed line). (a) Dispersion diagram. (b) Coalescence parameter.

In this structure, the two ports of the upper waveguide at both ends of the cavity are shorted, and the other two ports of the lower waveguide are connected to waveguide ports. The structure is therefore a two-port network; its S parameters are computed with Ansys HFSS and discussed. The quality factor of such a cavity is then computed from the S parameters and its behavior vesus the number of cells N will be a validation of the DBE condition.

Fig. 13 shows the magnitude of S parameters, each subfigure for a truncated line composed of a given number of cells, with and without losses. We show both f_d, the DBE frequency of the infinite periodic SIW line, and $f_{r,d}$, the resonance frequency of DBE cavities made of finite SIW lines with four different numbers of unit cells. The influence of the cavity length on the resonance frequency is the same observed in [12]: the resonance frequency $f_{r,d}$ is lower than the ideal DBE frequency f_d and it approaches f_d as the number of cells N increases. Despite the presence of losses, for all the lines

studied here (from four to eight cells), the resonance dips of $|S_{11}|$ are below -3 dB which is considered here the threshold to define the presence of a resonance. We show in Fig. 14 all the $|S_{11}|$ parameters of the four different cavities, which shows more clearly the shift in the resonant frequency as N increases and the presence of the resonances even in the lossy structures. The E-field distribution of an 8-cell line at DBE frequency is shown in Fig. 15 which fits the center-distributed rule of the "structured resonance" described in [26].

The Q-factor in lossless and lossy structures is shown in Fig. 16. We use the loaded Q-factor conventionally approximated as in [12]

$$Q = \frac{f_{r,d}}{\text{BW}} \qquad (3)$$

where the $f_{r,d}$ is the resonance closest to the DBE, BW is the 3-dB bandwidth of reflectance. This is a very meaningful calculation for high Q-factors. In Fig. 16, both the lossless and lossy Q-factors fit the expected N^5 scaling rule typical of DBE resonances. The difference between them becomes larger as N increases, thus predicting a limitation in the number of cells capable to sustain a DBE if losses are not compensated by active elements providing a suitable level of gain.

To summarize, DBE resonances have been observed in SIW cavities formed by up to eight unit cells, where the resonance is defined as a peak in $|S_{11}|$ below -3 dB. The Q-factor trend with respect to the number of cells N is not significantly modified by losses, which however affect the overall level of the quality factor.

At this point, we discuss the comparison in Table II relative to distinct unit-cell sizes (normalized with respect to the medium wavelength) and compare the quality factors of the main technologies who led to a DBE synthesis in the microwave range so far.

In terms of quality factors achieved with a given number of cells, the different technologies have similar performance. In terms of size, the SIW cell has an intermediate footprint between the circular waveguide (which has different applications anyway) and the microstrip lines. It is difficult to compare the level of losses since they heavily depend on the materials used. If we compare microstrip and SIW realizations, we can highlight that the SIW technology is more practical in staked PCB devices and is less sensitive to radiation losses at high frequencies. Furthermore, thanks to the absence of pins in the middle of a cell, our SIW cell is particularly suited to be modified with transversal slots as in slotted waveguides in order to realize a leaky-wave antenna based on an exceptional point [38]. The presence of the slot would act as an additional (radiation) loss (which is desired in this application) but would
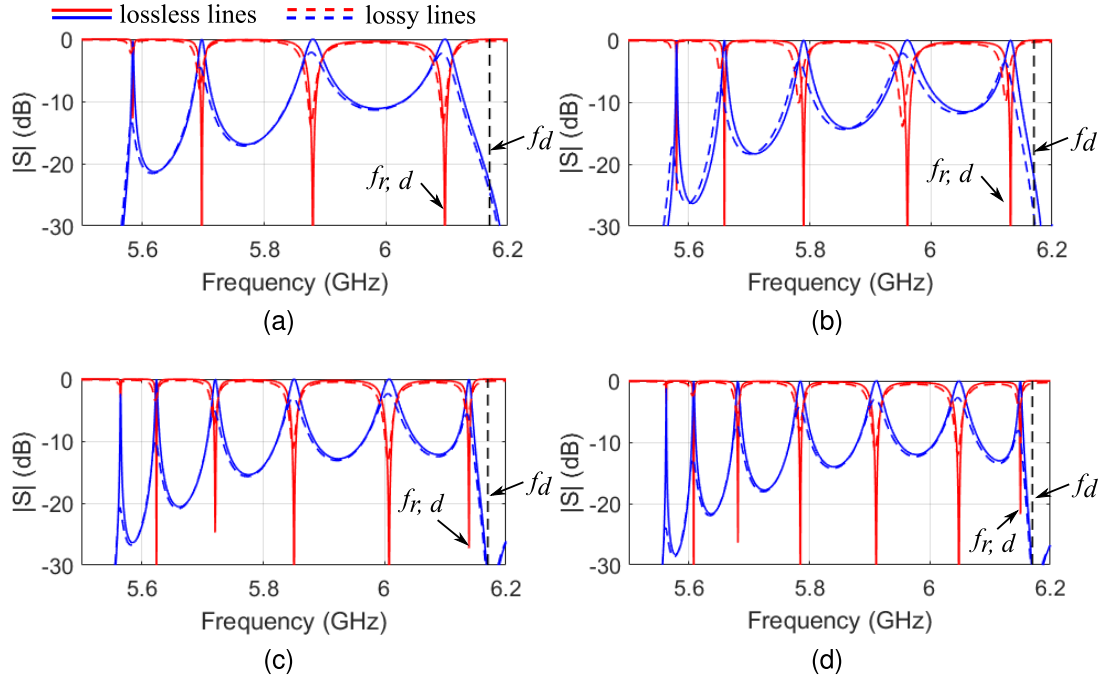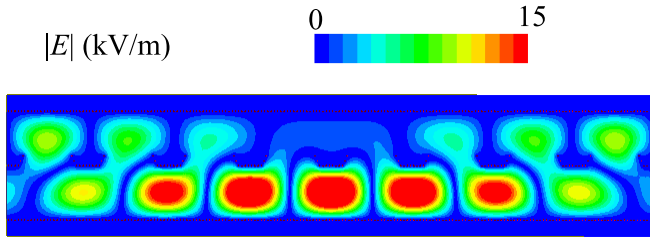
Fig. 13. S parameters of lossy truncated SIWs lines. S_{11} (red lines) and S_{21} (blue lines). (a) 5-cell, (b) 6-cell, (c) 7-cell, and (d) 8-cell.

TABLE II
COMPARISONS OF SIZES AND Q-FACTORS AMONG DBE TECHNOLOGIES

Technology	DBE freq. (GHz)	Unit-cell normalized size	Q (6 cells)
Circular waveguide (air filled) [11]	2.16	Length: 2.51, Diameter: 5.04	500
Coupled microstrips ($\varepsilon_r = 6.15$) [6]	2.8	0.58×0.34	not available
This work: "Corner cell" ($\varepsilon_r = 2.08$)	6.17	1.14×0.93	200
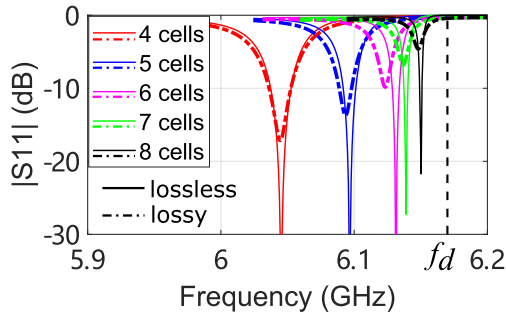
Fig. 14. Magnitude of S_{11} for different length "low-loss corner-cell" SIWs structures.

Fig. 16. Q-factor of "low-loss corner-cell" SIWs lines. Both lossless (red-circle mark) and lossy (blue-triangle mark) situations are considered. The scaling of Q-factor fits a N^5 law.

Fig. 15. E-field distribution of 8-cell truncated SIWs of "low-loss corner-cell."

not perturb the geometry as much as a modification meant to induce radiation into a microstrip line. Importantly, the lateral SIW size would not increase once slots are etched, while this would likely happen if a microstrip is made to radiate.
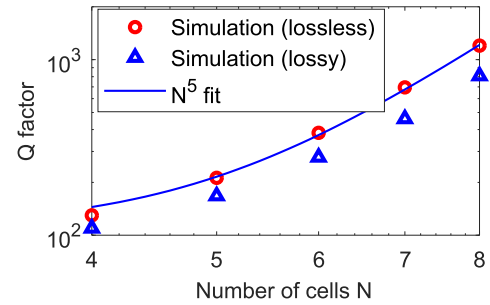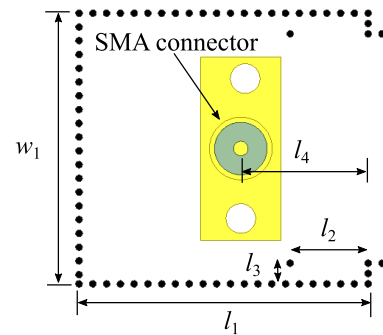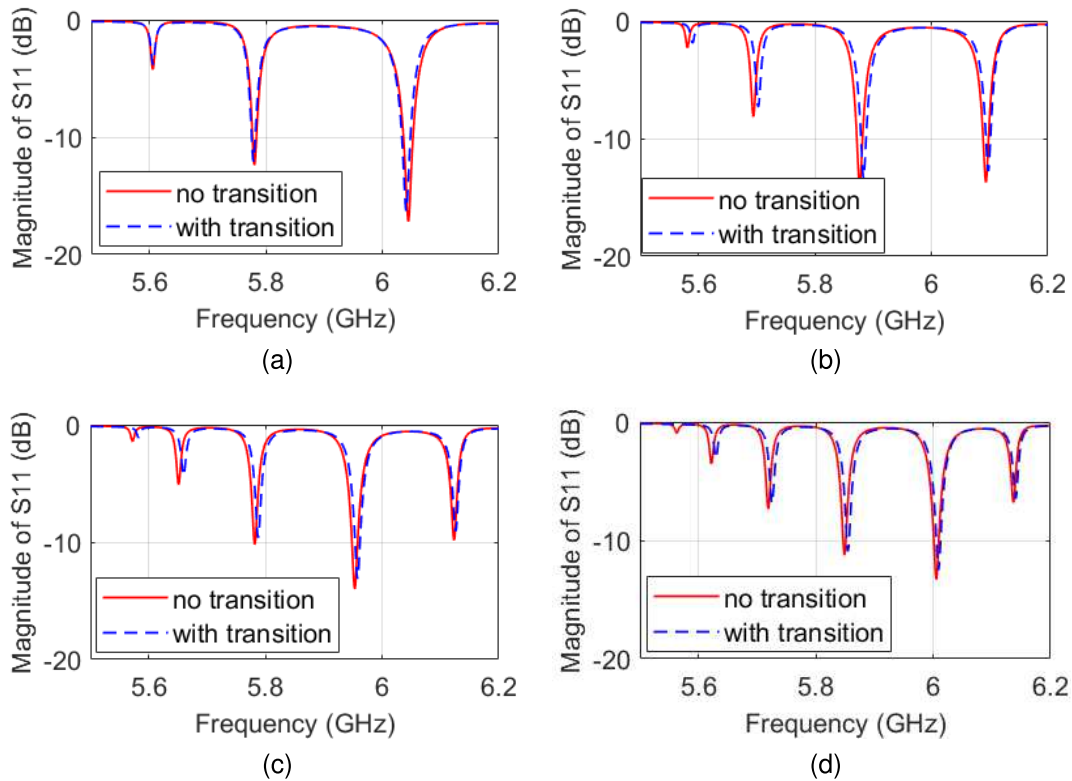

Fig. 17. SMA-SIW transition.

Fig. 18.   Negligible influence of SMA-SIW transition on $|S_{11}|$ of "low-loss corner-cell" lines. (a) 4-cell line. (b) 5-cell line. (c) 6-cell line. (d) 7-cell line. The "no transition" results (red solid lines) are obtained with ideal waveguide ports. The "with transition" results (blue dashed lines) are obtained with the SMA-SIW transition.

C. Design of Feeding Transitions for Truncated SIWs-DBE Lines

An SMA-SIW transition [39] is here implemented into the SIW-DBE lines. The advantage of this transition is its compact size and nonradiative characteristic. The SMA to SIW transition is shown in Fig. 17 where the substrate is the same used in the previous SIW cavity (Neltec NY9208, $\epsilon_r = 2.08$, loss tangent is 6×10^{-4} and thickness is 1.524 mm). The relevant dimensions shown in the figure are $w_1 = 23.6$ mm, $l_1 = 25.2$ mm, $l_2 = 6.8$ mm, $l_3 = 1.8$ mm, $l_4 = 11.1$ mm.

The magnitude of S_{11} of the truncated SIW lines fed through the SMA-SIW transitions is shown in Fig. 18, which shows a perfect agreement with the results obtained in Section III-B with the ideal waveguide ports. In conclusion, the shapes and frequencies of the DBE resonances are not altered by the presence of the transitions.

D. Experimental Results

In this section, we validate the analyses of Section III-C by showing the measurements of fabricated SIW-DBE cavity designs. For the fabrication of the SIW structures we have used a mechanical milling machine (LPKF ProtoMat S64) to drill the vias [Fig. 19(a)]. Then, the vias were metallized with an LPKF metallization paste (a rubber scraper was used to push the paste inside the vias and the board was heated in an oven to solidify the paste, see Fig. 19(b)]. At last, the SMA connectors were soldered and the final prototypes are shown in Fig. 19(b). Due to the size limitation of the milling machine, truncated lines up to six cells have been realized.

In Fig. 20(a)–(c), the S parameters of 4-, 5-, 6-cell SIW lines are presented. The measurement results are compared

Fig. 19.   Fabricated "low-loss corner-cell" SIWs lines. (a) Drilling details. (b) Final prototypes of 4-cell, 5-cell, and 6-cell "low-loss corner-cell" SIWs lines. The white part is the metallic paste.

with the lossy models simulated with Ansys HFSS, including transitions and SMA connectors, in Section III-C. The measured curves fit the simulation results very well, confirming in the fabricated prototypes the existence of the DBE resonance, approaching as expected the ideal DBE frequency as the number of cells increases. We can notice only a slight frequency shift of the DBE resonance in the range from 0.01 to 0.018 GHz between the measurements and the simulation results, likely caused by fabrication tolerances. Regarding the magnitudes of the resonant dips in the S parameters, the 4-cell measurement results fit very well with the simulation results. With the increase of the number of cells, small differences in the minimal dip values of $|S_{11}|$ appear. This can be related to different conductive losses associated with the metallic paste used for the vias, or to losses higher than expected in the copper or dielectric, or to small matching differences due to tolerances. Based on the S parameters measurements, we obtain the Q-factors in Fig. 20(d). The measured Q-factors
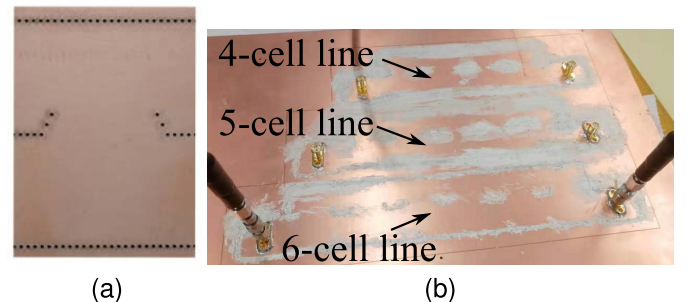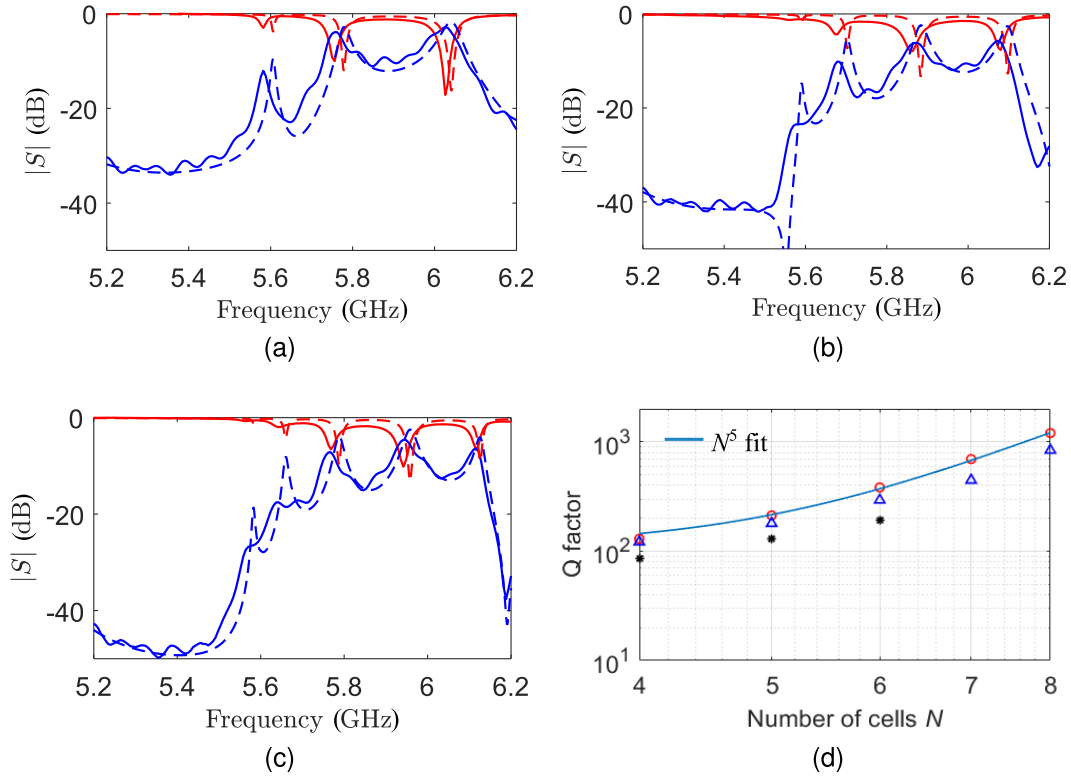
Fig. 20. Measurements of "low-loss corner-cell" SIWs lines. (a) *S* parameters of 4-cell truncated line. Measurement results: solid lines. Simulation results: dashed lines. S_{11}: red lines. S_{21}: blue lines. (b) *S* parameters of 5-cell truncated line. (c) *S* parameters of 6-cell truncated line. (d) Loaded *Q*-factor, computed with (3), versus the number of cells *N*. The resonance frequency $f_{r,d}$ and the bandwidth BW are computed from the magnitude of S_{11}. Lossless lines without transition: (red circles), lossy lines with SMA-SIW transition: (blue triangles), experimental results (black dots).

are slightly below the simulated ones, indicating that real losses are slightly higher than the simulated ones. However, the *Q*-factor still increases as expected following the same trend of the simulated results, thus confirming the excitation of DBE resonances and the correctness of the design.

IV. CONCLUSION

We have proposed three different unit cells capable to support a DBE condition in an SIW structure for the first time. Notably, the "corner cell" design has an interesting topology which is robust to the geometrical perturbation and suffers less of dielectric losses. Furthermore, one single geometrical parameter allows to tune the resonance frequency by keeping a DBE condition. This unit cell was therefore chosen to realize truncated SIW lines which present the typical characteristics of DBE, i.e., the giant resonances and the fast increase of *Q*-factor. The prototypes of the truncated resonators has been fabricated and the measurements of *S* parameters fit well with the simulation results thus validating the analyses and the designs.

Resonant DBE cavities can have multiple applications, for example in very stable oscillators [25], distributed oscillators [29] and pulse generators [26]. By virtue of the placement of the vias, the periodic line is amenable to be opened at its middle with radiating slots to realize a directive leaky-wave antenna extremely selective in frequency. The peculiarity of these antennas would be their extreme tunability in beam direction and beamwidth [38] that can be used either

for sensing or in directional finding. The performance of the DBE cavities depends on the length of the structure (number of cells). Typically, once the cavity is long enough (in our case $N \geq 5$), a distributed gain can be added along the line suitably tuned to compensate material losses as shown in other similar realizations.

REFERENCES

[1] A. Figotin and I. Vitebskiy, "Frozen light in photonic crystals with degenerate band edge," *Phys. Rev. E, Stat. Phys. Plasmas Fluids Relat. Interdiscip. Top.*, vol. 74, no. 6, pp. 66613–66630, Dec. 2006.

[2] A. Figotin and I. Vitebskiy, "Gigantic transmission band-edge resonance in periodic stacks of anisotropic layers," *Phys. Rev. E, Stat. Phys. Plasmas Fluids Relat. Interdiscip. Top.*, vol. 72, no. 3, p. 36, Sep. 2005.

[3] D. Oshmarin *et al.*, "New oscillator concept based on band edge degeneracy in lumped double-ladder circuits," *IET Circuits, Devices Syst.*, vol. 13, no. 7, pp. 950–957, Oct. 2019.

[4] J. T. Sloan, M. A. K. Othman, and F. Capolino, "Theory of double ladder lumped circuits with degenerate band edge," *IEEE Trans. Circuits Syst. I, Reg. Papers*, vol. 65, no. 12, pp. 3–13, Jan. 2018.

[5] N. Apaydin, L. Zhang, K. Sertel, and J. L. Volakis, "Experimental validation of frozen modes guided on printed coupled transmission lines," *IEEE Trans. Microw. Theory Techn.*, vol. 60, no. 6, pp. 1513–1519, Jun. 2012.

[6] A. F. Abdelshafy, M. A. K. Othman, D. Oshmarin, A. T. Almutawa, and F. Capolino, "Exceptional points of degeneracy in periodic coupled waveguides and the interplay of gain and radiation loss: Theoretical and experimental demonstration," *IEEE Trans. Antennas Propag.*, vol. 67, no. 11, pp. 6909–6923, Nov. 2019.

[7] E. Irci, K. Sertel, and J. Volakis, "Unidirectional transmission characteristics of printed magnetic photonic crystals," in *Proc. AP-S Int. Symp.*, Jul. 2008, pp. 1–4.

[8] M. B. Stephanson, K. Sertel, and J. L. Volakis, "Frozen modes in coupled microstrip lines printed on ferromagnetic substrates," *IEEE Microw. Wireless Compon. Lett.*, vol. 18, no. 5, pp. 305–307, May 2008.

[9] F. Yazdi, D. Oshmarin, T. Mealy, A. T. Almutawa, A. Nikzamir, and F. Capolino, "Sixth-order degenerate band edge in coupled microstrip waveguides," *Phys. Rev. Appl.*, vol. 17, p. 064049, 2022.

[10] A. M. Zuboraj, B. K. Sertel, and C. J. L. Volakis, "Propagation of degenerate band-edge modes using dual nonidentical coupled transmission lines," *Phys. Rev. Appl., Gen. Phys.*, vol. 7, no. 6, pp. 64030–64040, Jun. 2017.

[11] M. A. K. Othman and F. Capolino, "Demonstration of a degenerate band edge in periodically-loaded circular waveguides," *IEEE Microw. Wireless Compon. Lett.*, vol. 25, no. 11, pp. 700–702, Nov. 2015.

[12] M. A. K. Othman, X. Pan, Y. Atmatzakis, and C. G. Christodoulou, "Experimental demonstration of degenerate band edge in metallic periodically loaded circular waveguide," *IEEE Microw. Theory Techn.*, vol. 65, no. 11, pp. 4037–4045, Nov. 2017.

[13] M. G. Wood, J. R. Burr, and R. M. Reano, "Degenerate band edge resonances in periodic silicon ridge waveguides," *Opt. Lett.*, vol. 40, no. 11, p. 2493, Jun. 2015.

[14] J. R. Burr and R. M. Reano, "Zero-coupling-gap degenerate band edge resonators in silicon photonics," *Opt. Exp.*, vol. 23, no. 24, p. 30933, Nov. 2015.

[15] M. Y. Nada, M. A. K. Othman, O. Boyraz, and F. Capolino, "Giant resonance and anomalous quality factor scaling in degenerate band edge coupled resonator optical waveguides," *J. Lightw. Technol.*, vol. 36, no. 14, pp. 3030–3039, Jul. 15, 2018.

[16] M. Y. Nada, M. A. K. Othman, and F. Capolino, "Theory of coupled resonator optical waveguides exhibiting high-order exceptional points of degeneracy," *Phys. Rev. B, Condens. Matter*, vol. 96, no. 18, Nov. 2017, Art. no. 184304.

[17] C. Löcker, K. Sertel, and J. L. Volakis, "Emulation of propagation in layered anisotropic media with equivalent coupled microstrip lines," *IEEE Microw. Wireless Compon. Lett.*, vol. 16, no. 12, pp. 642–644, Dec. 2006.

[18] S. Yarga, K. Sertel, and J. L. Volakis, "Finite degenerate band edge crystals using barium titanate-alumina layers emulating uniaxial media for directive planar antennas," in *Proc. IEEE Antennas Propag. Soc. Int. Symp.*, Honolulu, HI, USA, Jun. 2007, pp. 1317–1320.

[19] G. Mumcu, K. Sertel, and J. L. Volakis, "Miniature antenna using printed coupled lines emulating degenerate band edge crystals," *IEEE Trans. Antennas Propag.*, vol. 57, no. 6, pp. 1618–1624, Jun. 2009.

[20] S. Yarga, K. Sertel, and J. L. Volakis, "Degenerate band edge crystals for directive antennas," *IEEE Trans. Antennas Propag.*, vol. 56, no. 1, pp. 119–126, Jan. 2008.

[21] S. Yarga, K. Sertel, and J. L. Volakis, "A directive resonator antenna using degenerate band edge crystals," *IEEE Trans. Antennas Propag.*, vol. 57, no. 3, pp. 799–803, Mar. 2009.

[22] M. A. K. Othman and F. Capolino, "Coupled transmission line array antennas with exceptional points of degeneracy," in *Proc. IEEE Int. Symp. Antennas Propag., USNC/URSI Nat. Radio Sci. Meeting*, Jul. 2017, pp. 57–58.

[23] A. F. Abdelshafy, M. A. K. Othman, F. Yazdi, M. Veysi, A. Figotin, and F. Capolino, "Electron-beam-driven devices with synchronous multiple degenerate eigenmodes," *IEEE Trans. Plasma Sci.*, vol. 46, no. 8, pp. 3126–3138, Aug. 2018.

[24] F. Yazdi, M. A. K. Othman, M. Veysi, A. Figotin, and F. Capolino, "A new amplification regime for traveling wave tubes with third-order modal degeneracy," *IEEE Trans. Plasma Sci.*, vol. 46, no. 1, pp. 43–56, Jan. 2018.

[25] D. Oshmarin, A. F. Abdelshafy, A. Nikzamir, M. M. Green, and F. Capolino, "Experimental demonstration of a new oscillator concept based on degenerate band edge in microstrip circuit," 2021, *arXiv:2109.07002*.

[26] V. A. Tamma, A. Figotin, and F. Capolino, "Concept for pulse compression device using structured spatial energy distribution," *IEEE Trans. Microw. Theory Techn.*, vol. 64, no. 3, pp. 742–755, Mar. 2016.

[27] N. Gutman, A. A. Sukhorukov, F. Eilenberger, and C. M. de Sterke, "Bistability suppression and low threshold switching using frozen light at a degenerate band edge waveguide," *Opt. Exp.*, vol. 20, no. 24, p. 27363, Nov. 2012.

[28] M. Veysi, M. A. K. Othman, A. Figotin, and F. Capolino, "Degenerate band edge laser," *Phys. Rev. B, Condens. Matter*, vol. 97, no. 19, May 2018, Art. no. 195107.

[29] A. F. Abdelshafy, D. Oshmarin, M. A. K. Othman, M. M. Green, and F. Capolino, "Distributed degenerate band edge oscillator," *IEEE Trans. Antennas Propag.*, vol. 69, no. 3, pp. 1821–1824, Mar. 2021.

[30] X.-P. Chen and K. Wu, "Substrate integrated waveguide filter: Basic design rules and fundamental structure features," *IEEE Microw. Mag.*, vol. 15, no. 5, pp. 108–116, Jul. 2014.

[31] T. Zheng, M. Casaletti, A. F. Abdelshafy, F. Capolino, Z. Ren, and G. Valerio, "Design of substrate integrated waveguides supporting degenerate band-edge resonances," in *Proc. 13th EuCAP Conf.*, 2019, pp. 1–3.

[32] T. Zheng, M. Casaletti, Z. Ren, A. F. Abdelshafy, F. Capolino, and G. Valerio, "High-Q substrate-integrated-waveguide resonator with degenerate band edge," in *Proc. Int. Conf. Electromagn. Adv. Appl. (ICEAA)*, Sep. 2019, p. 0836.

[33] T. Zheng, M. Casaletti, A. F. Abdelshafy, F. Capolino, Z. Ren, and G. Valerio, "Degenerate band edge resonances in air-filled substrate integrated waveguide," in *Proc. 14th Eur. Conf. Antennas Propag. (EuCAP)*, Mar. 2020, pp. 1–4.

[34] F. Mesa, G. Valerio, R. Rodriguez-Berral, and O. Quevedo-Teruel, "Simulation-assisted efficient computation of the dispersion diagram of periodic structures: A comprehensive overview with applications to filters, leaky-wave antennas and metasurfaces," *IEEE Antennas Propag. Mag.*, vol. 63, no. 5, pp. 33–45, Oct. 2021.

[35] V. Laude, J. M. Escalante, and A. Martínez, "Effect of loss on the dispersion relation of photonic and phononic crystals," *Phys. Rev. B, Condens. Matter*, vol. 88, no. 22, Dec. 2013, Art. no. 224302.

[36] D. Deslandes and K. Wu, "Accurate modeling, wave mechanisms, and design considerations of a substrate integrated waveguide," *IEEE Trans. Microw. Theory Techn.*, vol. 54, no. 6, pp. 2516–2526, Jun. 2006.

[37] M. Bozzi, L. Perregrini, and K. Wu, "Modeling of conductor, dielectric, and radiation losses in substrate integrated waveguide by the boundary integral-resonant mode expansion method," *IEEE Trans. Microw. Theory Techn.*, vol. 56, no. 12, pp. 3153–3161, Dec. 2008.

[38] M. A. K. Othman and F. Capolino, "Theory of exceptional points of degeneracy in uniform coupled waveguides and balance of gain and loss," *IEEE Trans. Antennas Propag.*, vol. 65, no. 10, pp. 5289–5302, Oct. 2017.

[39] A. Morini, M. Farina, C. Cellini, T. Rozzi, and G. Venanzoni, "Design of low-cost non-radiative SMA-SIW launchers," in *Proc. 36th Eur. Microw. Conf.*, Sep. 2006, pp. 526–529.

Tianyu Zheng (Student Member, IEEE) received the M.S. degree in electrical engineering from the Huazhong University of Science and Technology, Wuhan, China, in 2017, and the Ph.D. degree in electrical engineering from the Laboratoire de Génie électrique et électronique de Paris (GeePs), Sorbonne Université, Paris, France, in 2021.

He is currently a Research Associate with the Institute of Electrical Engineering, Chinese Academy of Sciences, Beijing, China. His current research interests include numerical methods in electromagnetics and modeling of electrical devices.

Massimiliano Casaletti (Senior Member, IEEE) was born in Siena, Italy, in 1975. He received the Laurea degree in telecommunications engineering and the Ph.D. degree in information engineering from the University of Siena, Siena, Italy, in 2003 and 2007, respectively.

From September 2003 to October 2005, he was with the Research Center MOTHESIM, Les Plessis Robinson, Paris, France, under EU Grant RTN-AMPER (Application of Multiparameter Polarimetry). He has been a Research Associate with the University of Siena, from November 2006 to October 2010, and a Post-Doctoral Researcher with the Institut d'Electronique et des Télécommunications de Rennes (IETR), University of Rennes 1, Rennes, France, from November 2010 to August 2013. He is currently an Associate Professor with Sorbonne Université, Paris, France. His research interests include numerical methods for electromagnetic (scattering, antennas, and microwave circuits), metasurface structures, field beam expansion methods, and electromagnetic band-gap structures.

Ahmed F. Abdelshafy (Student Member, IEEE) was born in Egypt in 1991. He received the Ph.D. degree in electrical engineering from the University of California, Irvine, CA, USA, in 2021.

From 2012 to 2016, he has been a Faculty Member with the Department of Electronics and Electrical Communications Engineering, Cairo University, Cairo, Egypt. He is currently a Senior RFIC Engineer with Skyworks Solutions, Inc., Irvine. His research interests include high-power electromagnetic sources, microwave and terahertz generation, dispersion engineering, RF bandgap circuits and oscillators, computational electromagnetics, numerical methods including eigenmode projection techniques, and FDTD.

Zhuoxiang Ren (Senior Member, IEEE) received the B.Sc. degree from the Huazhong University of Science and Technology, Wuhan, China, in 1982, and the Ph.D. degree from the Insititut Polytechnique de Toulouse, Toulouse, France, in 1985.

His working experience includes both academic and industrial research and development in France and in USA. He is currently a Full Professor with Sorbonne University, Paris, France, where he conducts his research in the Group of Electrical Engineering Paris (GeePs). He has published over 200 refereed journal and international conference papers. He is a coauthor of two book chapters. His research interests include numerical methods for electromagnetic and multiphysics problems and modeling and simulation of electrical and electronic devices and systems.

Dr. Ren has been awarded a Bronze Medal of CNRS in France in 1996.

Filippo Capolino (Fellow, IEEE) received the Laurea *(cum laude)* and Ph.D. degrees in electrical engineering from the University of Florence, Florence, Italy, in 1993 and 1997, respectively.

From 1997 to 1999, he was a Fulbright and then a Post-Doctoral Fellow with the Department of Aerospace and Mechanical Engineering, Boston University, Boston, MA, USA. From 2000 to 2001, part of 2005 and in 2006, he was a Research Assistant Visiting Professor with the Department of Electrical and Computer Engineering, University of Houston, Houston, TX, USA. From 2002 to 2008, he was an Assistant Professor with the Department of Information Engineering, University of Siena, Siena, Italy. He has been a Visiting Professor with the Fresnel Institute, Marseille, France, in 2003, and the Centre de Recherche Paul Pascal, Bordeaux, France, in 2010. He is currently a Professor with the Department of Electrical Engineering and Computer Science, University of California, Irvine, CA, USA. In 2022, he held the title of Cathedra of Excellence with the University of Carlos III, Madrid, Spain, for six months. His current research interests include metamaterials and their applications, electron beam devices, antennas, sensors in both microwave and optical ranges, plasmonics, microscopy, wireless systems, millimeter wave chip-integrated antennas, and applied electromagnetics in general.

Dr. Capolino received the R. W. P. King Prize Paper Award from the IEEE Antennas and Propagation Society for the Best Paper of the Year 2000, by an author under 36. He was the Founder and the Coordinator of the EU Doctoral Programs on Metamaterials from 2004 to 2009. From 2002 to 2008, he served as an Associate Editor for the IEEE TRANSACTIONS ON ANTENNAS AND PROPAGATION. He is the Editor of the *Metamaterials Handbook* (Boca Raton, FL, USA: CRC Press, 2009).

Guido Valerio (Senior Member, IEEE) received the M.S. degree *(cum laude)* in electronic engineering and the Ph.D. degree in electromagnetics from La Sapienza University, Rome, Italy, in 2005 and 2009, respectively.

From February to August 2008, he was a Visiting Scholar with the University of Houston, Houston, TX, USA. From 2011 to 2014, he was a Researcher with the Institute d'Electronique et de Télécommunications de Rennes (IETR), Rennes, France. Since September 2014, he has been with Sorbonne Université, Paris, France, where he is currently a Professor. His scientific interests involve periodic Green's function computation, modal properties of multilayered structures, full-wave methods for SIW, and modeling and design of periodic structures with higher symmetries.

Dr. Valerio was a recipient of the Leopold B. Felsen Award for Excellence in Electrodynamics in 2008, the Barzilai Prize for the best paper at the National Italian Congress of Electromagnetism (XVIII RiNEm) in 2010, and the RMTG Award for Junior Researchers presented at the IEEE Antennas and Propagation Society Symposium, Memphis, TN, USA, in 2014. In 2018 and 2020, he was a coauthor of the best papers in Electromagnetic and Antenna theory at the European Conference on Antennas and Propagation. In 2022, he was a coauthor of the Best Student Paper Award at the 16th European Conference on Antennas and Propagation. He is the Main Chair of the COST Action SyMat on Future communications with higher symmetric engineered artificial materials. He is currently serving as an Associate Editor for the IEEE TRANSACTIONS ON ANTENNAS AND PROPAGATION and IEEE ACCESS.